

Probabilistic sensitivity analysis to understand the influence of micromechanical properties of wood on its macroscopic response

P.O. Hristov^{a,*}, F.A. DiazDelaO^a, E.I. Saavedra Flores^b, C.F. Guzmán^b, U. Farooq^c

^a*Institute for Risk and Uncertainty, School of Engineering, University of Liverpool, Liverpool L69 7ZF, United Kingdom*

^b*Departamento de Ingeniería en Obras Civiles, Universidad de Santiago de Chile, Av. Ecuador 3659, Estación Central, Santiago, Chile*

^c*Parker Hannifin Manufacturing (UK) Ltd*

Abstract

This paper investigates the influence of the uncertainty in different micromechanical properties on the variability of the macroscopic response of cross-laminated timber plates, by means of a probabilistic sensitivity analysis. Cross-laminated timber plates can be modelled using a multiscale finite element approach which although suitable, suffers from high computational cost. Investigating parametric importance can incur considerable time penalty since conventional sensitivity analysis relies on a large number of code evaluations to produce accurate results. In order to address this issue, we build a statistical approximation to the code output and use it to perform sensitivity analysis. We investigate the effect of a collection of parameters on the density and Young's moduli of wood. Additionally, the influence on the response of cross-laminated timber plates subject to bending, in-plane shear

*Corresponding author. Tel. +44(0)747 461 42 87
Email address: p.hristov@liv.ac.uk (P.O. Hristov)

and compression loads is investigated due to its relevance within the engineering community. The presented results provide a practical insight into the importance of each micromechanical parameter, which allows research effort to be focused on the important wood properties.

Keywords: Probabilistic sensitivity analysis, Gaussian process emulation, Cross laminated timber, Multi-scale analysis, Finite elements

1. Introduction

In recent years, considerable attention has been paid to the investigation of wood at multiple length scales. At microscopic levels, wood shows remarkable features, such as its highly organised hierarchical design, its ability to deflect microcracks which results in an increased fracture toughness, and its lightweight and excellent thermal and acoustic insulation characteristics due to its porous microstructure. At very large scales, the above properties, combined with its reduced environmental impact, make wood to be an ideal candidate for building applications. In particular, cross-laminated timber (CLT) has been increasingly spreading in Europe and North America over the last decade as a novel prefabricated building system [1]. CLT panels are composite structures made up of several layers of boards stacked crosswise and glued together on their faces, as can be seen in Figure 1.

[Figure 1 about here.]

The main advantages of CLT are its fast and efficient on-site installation, its favourable seismic performance, its ability to self-protect against fire and its excellent strength [2].

18 Despite the above advantages, the computational modelling of CLT, and
19 in general timber structures, still represents a very challenging task. This can
20 be attributed to the highly heterogeneous macroscopic properties of wood.
21 One possible approach to tackle this problem is to predict the macroscopic
22 response using the mechanical information coming from its microstructure.
23 This task can be achieved by means of the finite element (FE) based mul-
24 tiscala modelling technique [3]. Considerable effort has been devoted to the
25 computational modelling of timber structures [4, 5, 6, 7], but the complete
26 understanding of the mechanical properties of this material at small spatial
27 scales is still an open issue.

28 The micromechanical properties of wood can be uncertain due to the lack
29 of knowledge or because of measurement errors at such small length scales.
30 As these properties are crucial to develop reliable predictive models, the un-
31 certainty in their values must be taken into account. Recently, Saavedra
32 Flores et al. [8, 9] considered the uncertainty in the micromechanical param-
33 eters of a multiscale model for wood. This uncertainty was propagated to the
34 macro-scale, giving rise to uncertain macroscopic properties. In this new pa-
35 per, we continue the line of development started in the above references [8, 9].
36 By means of a probabilistic sensitivity analysis, we investigate the influence
37 of uncertainty in different microscopic properties on the variability of the
38 macroscopic response of wood. Probabilistic sensitivity analysis (SA) relies
39 on a large number of expensive code evaluations to produce accurate results.
40 In order to tackle the high computational cost associated with the analysis,
41 we build a more affordable surrogate of the code and use it to perform the
42 numerical studies. There are a number of methodologies for approximating

43 the output of expensive codes, see *e.g.* [10]. One particular approach is
44 Gaussian process emulation (GPE), which builds a statistical approximation
45 to the output of the code. Using this technique we investigate the extent
46 to which different micromechanical parameters influence the macroscopic re-
47 sponse of wood. Due to its relevance within the engineering community, we
48 also explore the influence on the response of CLT plates subject to bending,
49 in-plane shear and compression loads. Once the relative importance of dif-
50 ferent parameters is known, the information can be used to either reduce the
51 computational cost of the model by fixing the least influential variables, or
52 to maximize the reduction in response uncertainty by conducting research
53 on the important wood properties.

54 The rest of the paper is organized as follows: Section 2 outlines the rel-
55 evant wood properties and corresponding modelling strategies. Section 3
56 introduces the basics of probabilistic sensitivity analysis and Gaussian pro-
57 cess emulation. Section 4 presents the micro-macro study, in which the effect
58 of the micro parameters on each macro parameter is measured. Section 5
59 provides an interpretation of the results from the previous section and finally
60 Section 6 draws the main conclusions of the presented work.

61 **2. Multi-scale modelling**

62 The multiscale modelling of timber is described in this section. A com-
63 putational homogenisation approach is adopted to capture the hierarchical
64 nature of wood at different length scales. Here, four different spatial scales are
65 considered. These are the nanometer, micrometer, millimeter and the struc-
66 tural scales. For further details on the present homogenisation approach, we

67 refer, for instance, to Saavedra Flores et al.[11].

68 *2.1. Relevant wood micromechanical parameters*

69 At nanometer levels, wood contains three basic constituents: cellulose,
70 hemicellulose and lignin [12]. These three fundamental constituents form the
71 wood cell-wall composite material whose basic unit building block is called
72 microfibril. This composite comprises reinforcing cellulose fibrils oriented
73 mainly in a single direction (in almost the whole cell-wall volume) periodically
74 embedded in a softer matrix.

75 The specific angle of the microfibrils with respect to the longitudinal
76 axis of the wood cell is typically called microfibril angle, *MFA*. The volume
77 fraction of cellulose f_c is defined as the volume of cellulose with respect to
78 the total volume of the cell-wall composite. Similarly the volume fraction of
79 hemicellulose f_h relates the volume of hemicellulose. The reinforcing cellulose
80 is made up of periodic alternations of crystalline and amorphous fractions.
81 The degree of cellulose crystallinity f_{cc} is defined as the volume fraction of the
82 crystalline portion of cellulose with respect to the total volume of cellulose.
83 As the cellulose is a long and stiff polymeric fibre, the length of the crystalline
84 fraction is termed here L_{cc} .

85 The matrix of the cell-wall composite is made of hemicellulose and lignin
86 polymers. Hemicellulose is built up of sugar units and has little strength,
87 with mechanical properties highly sensitive to moisture changes. Lignin is
88 an amorphous and hydrophobic polymer and its main purpose is to cement
89 the individual wood fibres together and to provide inter-fibre shear strength.

90 At the micrometer scale, the material can be represented by a periodic
91 arrangement of long slender tubular micro-fibres (or wood cells), oriented

92 nearly parallel to the axis of the stem. The cross-sections of each micro-fibre
 93 is (normally) hexagonal, and can be defined by means of four geometric pa-
 94 rameters. These are the tangential and radial dimensions of the hexagonal
 95 cross-section, denoted here as T and R (along the tangential and radial direc-
 96 tions of wood), respectively, the thickness of the cell-wall, t_c , and the angle
 97 θ (whose value can be, for instance, 0° for a rectangular cross-section, or 30°
 98 for a regular hexagonal shape). In softwoods, wood fibres can be divided
 99 into *early-wood* and *late-wood*. The *early-wood* fibres are characterised by
 100 large diameters and thin cell-walls, whereas *late-wood* fibres are composed of
 101 narrow diameters with much thicker cell-walls. In order to avoid confusion,
 102 we use in this paper the following terminology to differentiate both types of
 103 cells. The variables T_p , R_p and t_{cp} refer to the tangential and radial dimen-
 104 sions and thickness of *early-wood* fibres. Similarly, T_v , R_v and t_{cv} refer to the
 105 tangential, radial and thickness dimensions of *late-wood* fibres. Given the
 106 little information reported on the distinction of θ between *early-wood* and
 107 *late-wood*, such an angle is assumed to be the same for both types of cells.

108 At the scale of a few millimeters wood is represented by the growth rings,
 109 typically found in the cross-section cut through the trunk of a tree. Within
 110 a growth ring, the volume fraction of *early-wood* fibres with respect to the
 111 total volume of growth ring is denoted as P_{ew} . For further information about
 112 the morphology and composition of wood at microscopic levels, we refer, for
 113 instance, to [13, 14]. The final macroscopic or structural scale is represented
 114 by the periodic repetition of the growth rings which form the base material.

115 Summarizing, 13 micromechanical parameters are defined. Four at the
 116 nanometer scale (MFA , f_c , f_h and f_{cc}), eight at the micrometer scale (t_c ,

117 θ , T_p , R_p , t_{cp} , T_v , R_v and t_{cv}) and one at the millimeter scale (P_{ew}).

118 2.2. Macroscopic parameters

119 The general procedure consists of building a material model for wood by
120 homogenising the three material scales described in the previous section (at
121 the level of the microfibril, wood fibres and growth rings). With this model
122 at hand, we can predict the response of any (macroscopic) timber structure
123 (that is, the structural scale).

124 In this study, we choose two types of structural configurations. First, we
125 analyse a timber plate of length of 2.4 m (parallel direction to wood fibres),
126 width of 1.2 m (perpendicular direction to wood fibres), and thickness of 4 cm.
127 We note that the general dimensions of 1.2 m by 2.4 m belong to a standard
128 geometry adopted typically for the experimental testing of structural panels
129 [15, 16, 17]. The plate is subject to four-point bending along the length and
130 width of the panel. From these analyses we obtain the longitudinal and trans-
131 verse Young's moduli for wood, E_0 and E_{90} , respectively. Second, we analyse
132 a CLT plate. The motivation of choosing CLT for this study is because of its
133 increasing use worldwide as a promising prefabricated construction system
134 [11]. The CLT plate consists of three layers of boards stacked crosswise and
135 glued together on their faces. Each layer is 4 cm of thick, with a length of
136 2.4 m and a width of 1.2 m (that is, the first configuration described above).
137 Thus, the total thickness of the CLT plate is 12 cm. The outer layers are
138 made of timber members oriented in the long direction of the panel (that is,
139 the strong direction). The central layer is made of members oriented in the
140 short (or weak) direction. The CLT plate is subject to three-point bending
141 along the strong direction, in-plane shear loading and compression parallel to

142 wood fibres in the outer layers. From these analyses, we obtain the bending
143 stiffness K_{bend} , the in-plane shear stiffness K_{sh} and the axial stiffness K_{comp}
144 of the CLT plate. For further details on these stiffness components, we refer
145 to [11]. In addition, we compute the macroscopic density of the material ρ .
146 The above six macroscopic parameters (ρ , E_0 , E_{90} , K_{bend} , K_{comp} and K_{sh}) are
147 selected because of their relevance in the day-to-day practice of analysis and
148 design of timber structures, particularly in the context of CLT structures.

149 *2.3. Modelling of macro and micro-scales*

150 Multi-scale models enable specifying the relationships between physical
151 variables observed at different length scales. These are of particular impor-
152 tance in the study of heterogeneous materials with hierarchical microstruc-
153 tures in which the macroscopic response of the material can be predicted
154 from the information coming from the microscopic (or lower) level.

155 In the present multiscale constitutive theory, each material scale is asso-
156 ciated with a microstructure whose most statistically relevant features are
157 incorporated within a representative volume element (RVE). This RVE is
158 assumed to have a (microscopic) characteristic length much smaller than the
159 macro-continuum, and at the same time, a size large enough to capture the
160 microscopic heterogeneities in an averaged sense. This multiscale method-
161 ology has proven to be successful to reproduce the mechanical behaviour of
162 materials at several length scales. As described at the beginning of Section 2,
163 four spatial scales can be identified. Three of them represent material scales,
164 and a fourth is associated with the structural scale.

165 Depending on the kinematic constraints imposed in the RVE, several
166 classes of multiscale models can be defined. Here, we choose the periodic

167 boundary displacement fluctuations multiscale model [18], which is typically
168 used to model periodic media, like wood micro structures and several other
169 natural materials. The type of wood species chosen for this investigation is
170 radiata pine grown in Chile, which has several applications in building and
171 engineering structures.

172 Each spatial scale was modelled using the FE model with meshes depicted
173 in Figure 2. Note that all the FE meshes used in our computational sim-
174 ulations were obtained after a preliminary convergence study. The results
175 (omitted here for brevity) did not indicate a significant change of the simu-
176 lation outcomes for increasing mesh densities. Additionally, the same mesh
177 was used in previous works [2, 19] We also note that the first two material
178 scales (Figure 2(a), Figure 2(b), Figure 2(c)) have already been described
179 in [11] and therefore, we skip the details about their modelling. A typical
180 finite element mesh of the RVE chosen to describe the mechanical response
181 of the growth ring is shown in Figure 2(d). It consists of 288 nodes and 165
182 hexahedral elements. The turquoise colour represents the portion of mate-
183 rial calculated by the computational homogenisation of the *early-wood* RVE
184 shown in Figure 2(c), whereas the light brown colour shows the material ob-
185 tained by the homogenisation of the *late-wood* RVE shown in Figure 2(b).
186 The periodic repetition of the growth rings forms the base material for the
187 macroscopic or structural scale (in this case, the CLT panels). This scale
188 is modelled using the finite element mesh depicted in Figure 2(e) (for the
189 four-point bending) and 2(f) (for the three-point bending). The discretisa-
190 tion is the same in both figures, with 379 093 nodes and 345 600 SOLID45
191 elements. The computational homogenisation procedure described in this

192 section is implemented in the commercial software ANSYS [20].

193 [Figure 2 about here.]

194 **3. Probabilistic sensitivity analysis**

195 Being a representation of a complex natural process, it is expected that
196 the FE code will also be complex. Complexity of computer codes is mainly
197 associated with their high computational cost and the lack of an analyti-
198 cal expression of the input/output mapping i.e., the model is treated as a
199 *black box*. The multiscale FE model used in this paper is a deterministic
200 simulator. This means that the output is precisely the same, every time its
201 multidimensional input is given the same value. Despite this, micromechan-
202 ical parameters are physical quantities and as such come from some joint
203 probability distribution, $f_X(\mathbf{x})$ effectively making them an uncertain multi-
204 variate random variable, \mathbf{X} . This uncertainty is propagated to the output
205 through the simulator. Thus, the output $y = \eta(\mathbf{x})$ can be seen as a random
206 variable $Y = \eta(\mathbf{X})$, with its own probability distribution. Very often the
207 different inputs do not influence the output equally. Part of the computer-
208 based investigation of the physical process is determining the influence of the
209 uncertainty in the different inputs, or sets of inputs, on the variability of the
210 output. This process is known as probabilistic *sensitivity analysis* (SA).

211 There are two main types of sensitivity analyses, namely local (LSA) and
212 global (GSA). LSA is concerned with determining the effect of small, local
213 perturbations in the parameter value around a given base point. A very
214 common local sensitivity approach is the one based on derivatives, namely
215 $\partial Y / \partial X_i$, where X_i is the i^{th} component of \mathbf{X} . The local method is not used

216 in the current investigation, since it fails to capture the effect of the inputs
217 when their values are arbitrarily chosen from the entire input domain. For
218 more detail on LSA see [21].

219 In order to fully explore the input space, GSA relies on a number of
220 points carefully spread according to some experimental design. There ex-
221 ists a variety of GSA techniques such as function decomposition in main
222 and higher order effects, regression coefficients and variance-based methods,
223 among others (see for example [21]).

224 3.1. Variance-based sensitivity analysis

225 Since the models of interest are deterministic, the variance of the output
226 random variable will be entirely due to the uncertainty in the input values.
227 This means that if one could learn the exact, true values of the inputs, the
228 variance of Y would be reduced to 0. This leads to the notion that fixing
229 one of the inputs X_i at a given value x_i and re-running the code will result
230 in Y having a lower variance. Let $\mathbb{V}_{\sim_i}[Y|X_i]$ be the conditional variance of
231 Y , taken over all factors, but X_i (denoted X_{\sim_i}) and given $X_i = x_i$. This
232 conditional variance can be used as a measure of how influential the fixed
233 parameter is. A severe drawback of this measure, however, is its dependence
234 on the location of the point x_i . This problem could be resolved by taking
235 the average of the conditional variance over all possible values of x_i , that is
236 $\mathbb{E}_i[\mathbb{V}_{\sim_i}[Y|X_i]]$. It is a well known fact in Probability theory that the variance
237 of a random variable can be decomposed as:

$$\mathbb{V}[Y] = \mathbb{E}_i[\mathbb{V}_{\sim_i}[Y|X_i]] + \mathbb{V}_i[\mathbb{E}_{\sim_i}[Y|X_i]] \quad (1)$$

238 Eq. (1) gives another important diagnostic - $\mathbb{V}_i[\mathbb{E}_{\sim i}[Y|X_i]]$ - *the first order*
 239 *effect* of X_i on Y . The associated normalised sensitivity measure, also known
 240 as a *Sobol' index* [22] is:

$$S_i = \frac{\mathbb{V}_i[\mathbb{E}_{\sim i}[Y|X_i]]}{\mathbb{V}(Y)} \quad (2)$$

241 A high value of the Sobol' index for the given variable, means that it is
 242 important, i.e. if it is fixed, there will be a significant reduction in the
 243 variance of Y .

244 Many practical models are of the so-called *non-additive* class. That is,
 245 the effect that individual inputs have on the variance cannot be separated
 246 to account for 100% of the output variance. Instead, interactions between
 247 individual inputs or sets of inputs will play an important role. To capture
 248 such effects, the *higher-order Sobol' indices* can be constructed:

$$S_p = \frac{\mathbb{V}_p[\mathbb{E}_{\sim p}[Y|\mathbf{X}_p]]}{\mathbb{V}(Y)} \quad (3)$$

249 where $p \subset \{1, \dots, d\}$ is a set of indices of all inputs under investigation. It
 250 can be shown that:

$$\sum_{i=1}^d S_i + \sum_{i<j}^d S_{i,j} + \sum_{i<j<k}^d S_{i,j,k} + \dots + S_{1,2,\dots,d} = 1 \quad (4)$$

251 where the summation is carried out over all d dimensions, which means that
 252 summing over all Sobol' indices recovers the full variance. Full analysis of the
 253 main effects of the model inputs and their respective interactions will result
 254 in Eq. (4) having $2^d - 1$ terms. This means that with relatively low num-
 255 ber of inputs, the summation components become too many to investigate

256 individually. Homma and Saltelli [23] introduced the *Total Sobol' index*:

$$S_{T_i} = \left(1 - \frac{\mathbb{V}_{\mathbf{X}_{\sim i}}[\mathbb{E}_{X_i}[Y|\mathbf{X}_{\sim i}]]}{\mathbb{V}(Y)} \right) \quad (5)$$

257 This measure captures the effect of the i -th input and all of its interactions,
258 by fixing all other inputs. It is true that $S_i \leq S_{T_i}$, due to interactions between
259 inputs. Equality can only arise in a perfectly additive model. An input is
260 said to be truly non-influential if and only if $S_{T_i} = 0$. In [24] the authors
261 have argued that a good, albeit non-exhaustive characterization of the input
262 influences is given by the set of first order and total Sobol' indices. This is
263 further discussed with the results presented in Section 4.

264 3.2. Gaussian process emulation

265 Simulators used to model complex scientific phenomena are usually very
266 computationally expensive. This is to say that a single evaluation of the
267 code's output at a given set of input values takes sufficiently long time, as
268 to prohibit any type of analysis which requires a large number of model
269 runs. The multiscale FE code used in this work is no exception. Since
270 sensitivity analysis relies on Monte Carlo (MC) approximations of integrals,
271 the estimators of the Sobol' indices will converge to their true value as the
272 number of points used to estimate them approaches infinity. Clearly, the
273 analysis cannot be carried out using the code directly. In such cases it is
274 common to use a less expensive approximation of the code output. These
275 approximations are widely known as *metamodels* or *emulators*. There is a
276 number of existing metamodelling techniques, but for the purposes of this
277 study, Gaussian process emulators (GPE) are used. Formally, the model

278 structure is expressed as:

$$\eta(\mathbf{x}) = h(\mathbf{x})^T \boldsymbol{\beta} + Z(\mathbf{x}) \quad (6)$$

279 where $\eta(\mathbf{x})$ is the simulator output as a function of its inputs, $h(\mathbf{x})^T$ is a
 280 known function of the inputs, $\boldsymbol{\beta}$ is a vector of unknown coefficients and $Z(\mathbf{x})$
 281 is a Gaussian process with zero mean, and covariance, $\sigma^2 c(\mathbf{x}, \mathbf{x}'; \psi)$. The
 282 function $h(\mathbf{x})$ should express any expert opinion about the form of the simu-
 283 lator output and together with the parameter $\boldsymbol{\beta}$ reflects its overall trend. In
 284 practice however, the trend is often taken to be constant as $h(\mathbf{x}) = 1$, charg-
 285 ing the Gaussian process in Eq. (6) with the responsibility of capturing the
 286 behaviour of the underlying function. In the formulation above, σ^2 is a scale
 287 parameter, $c(\mathbf{x}, \mathbf{x}'; \psi)$ is a known correlation function and ψ is a parameter
 288 specifying the behaviour of the correlation function. The parameters of the
 289 Gaussian process are also commonly referred to as *hyperparameters* [25] to
 290 distinguish them from the model parameters.

291 Using the GPE, a *posterior* probability distribution for the mean of the
 292 computer code's output can be constructed, conditional on a relatively small
 293 number of simulator runs with outputs \mathbf{y} and the estimated parameter values,
 294 $\hat{\boldsymbol{\theta}} = \{\hat{\beta}, \hat{\sigma}^2, \hat{\psi}\}$. It can be shown [26] that at a new unobserved set of input
 295 values, \mathbf{x}^* , the posterior distribution has the form of a multivariate Gaussian
 296 distribution:

$$\eta(\mathbf{x}^*) | \mathbf{y}, \hat{\boldsymbol{\theta}}, \sim \mathcal{N}(m(\mathbf{x}^*), C(\mathbf{x}^*, \mathbf{x}^*)) \quad (7)$$

297 with posterior predictive mean function:

$$m(\mathbf{x}^*) = \hat{\beta} + \mathbf{t}(\mathbf{x}^*)^T \mathbf{C}^{-1}(\mathbf{y} - \mathbf{1}\hat{\beta}) \quad (8)$$

298 and posterior predictive covariance function:

$$C(\mathbf{x}^*, \mathbf{x}'^*) = \hat{\sigma}^2(c(\mathbf{x}^*, \mathbf{x}^*) - \mathbf{t}(\mathbf{x}^*)^T \mathbf{C}^{-1} \mathbf{t}(\mathbf{x}'^*)) \quad (9)$$

299 In Eqs. (8) and (9) $\mathbf{C} \in \mathbb{R}^{n \times n}$ such that $C_{ij} = c(\mathbf{x}_i, \mathbf{x}_j)$, $\mathbf{t}(\mathbf{x}^*) \in \mathbb{R}^n$ such that
 300 $\mathbf{t}(\mathbf{x}^*) = (c(\mathbf{x}^*, \mathbf{x}_1), \dots, c(\mathbf{x}^*, \mathbf{x}_n))^T$ and $\mathbf{1} \in \mathbb{R}^n$ such that $\mathbf{1} = (1, \dots, 1)^T$. The
 301 process of estimating $\boldsymbol{\theta}$ (i.e. constructing $\hat{\boldsymbol{\theta}}$) from observed data is referred
 302 to as *training* and is very well described in [10] from a classical prospective
 303 or in [26, 27] from a Bayesian standpoint. Once the emulator is trained, its
 304 posterior distribution can be sampled many times at an affordable cost to
 305 provide data for various analyses.

306 4. Micro-Macro analysis

307 4.1. Gaussian process emulator validation

308 The micro-macro analysis deals with the investigation of relations be-
 309 tween the 13 microscopic properties and the 6 macromechanical parameters
 310 described in Section 2. The 6 macro parameters are analysed independently
 311 by fitting one Gaussian process per parameter. Therefore, the black-box
 312 function is of the form $M_j = \eta(m_1, \dots, m_{13})$, where the M_j is the j^{th} macro
 313 parameter and m_1, \dots, m_{13} are the micro parameters.

314 [Table 1 about here.]

315 Since the multiscale model is expensive, it should only be run as many times
 316 as necessary. When performing computer experiments it is common to apply
 317 the $10d$ rule [22] for selecting the size of the training sample for the GPE.

318 Therefore, 130 uniformly distributed points were selected via a Latin hy-
 319 percube sampling (LHS). LHS was chosen because it best represents each
 320 individual dimension. Another 60 LHS points were chosen as a validation
 321 set to check the quality of the GPE. The GPE was coded in MATLAB[®] and
 322 the model was run 190 times. The material properties of the model and the
 323 lower and upper bounds are retrieved from Saavedra Flores et al. [8, 11].
 324 Table 1 gives the ranges of the each micromechanical parameter. The val-
 325 ues were constrained in order to match physically possible values and the
 326 available experimental data. The properties are assumed to be stochasti-
 327 cally distributed as uniform random variables because they are susceptible
 328 to considerable variations when measured experimentally [11]. A genetic al-
 329 gorithm was used to perform a direct search for the optimal hyperparameter
 330 values and the mean and variance were calculated via maximum likelihood
 331 estimation (MLE) [10]. There are a variety of validation techniques, which
 332 could be used for identifying problems with the emulator (see for example
 333 [28]). Here we have used individual prediction errors which are represented
 334 by the normalised difference between the real and predicted values of each
 335 test point:

$$D_i^I = \frac{y_i - \mathbb{E}[\eta(\mathbf{x}_i^*)|\mathbf{y}]}{\sqrt{\mathbb{V}[\eta(\mathbf{x}_i^*)|\mathbf{y}]}} \quad (10)$$

336 where the expected value of the posterior distribution, $\mathbb{E}[\eta(\mathbf{x}_i^*)|\mathbf{y}]$ and its
 337 variance $\mathbb{V}[\eta(\mathbf{x}_i^*)|\mathbf{y}]$ are given in functional form in Eq. (8) and Eq. (9),
 338 respectively. If the emulator can accurately represent the simulator, these
 339 errors should have a standard *Student-t* distribution. With a large number of
 340 degrees of freedom the *Student-t* approaches a standard normal distribution
 341 and thus, any errors with absolute value greater than 2 (i.e. outside of the

342 95 % credible interval) can be considered local conflicts between emulator
343 and simulator. Patterns of errors lying outside the $[-2, 2]$ region could in-
344 dicate more serious problems. A useful visual validation tool is the plot of
345 predictions at the test points versus their true values. Figure 3 shows the
346 validation results for all 6 macro parameters. It can be seen that there is a
347 close correspondence between predictions and observations. Each point also
348 displays the 95% credible interval, which is based on the posterior predictive
349 variance. The individual prediction errors plotted against prediction values
350 are shown in Figure 4. All but a few of the errors lie within the desired
351 boundaries, which together with the plots in Figure 3 suggest that the emu-
352 lator is a valid representation of the simulator. Once the GPE was validated
353 the 60 points used for the process were added to the training sample and the
354 surface was refit based on all 190 points.

355 [Figure 3 about here.]

356 [Figure 4 about here.]

357 4.2. Calculation of Sobol' indices

358 As mentioned in Section 3.1, the calculation of Sobol' indices requires
359 the evaluation of both conditional and unconditional expectations and vari-
360 ances. These operations are associated with the calculation of a number of
361 integrals. In order to evaluate them, the integrals can be approximated by
362 Monte Carlo (MC) simulation. Since this is the case, a relatively large sam-
363 ple size is required to achieve reasonably accurate estimation results. This
364 is often a problem because, coupled with the computational complexity of
365 most scientific and engineering codes, extensive sampling results in a very

366 costly sensitivity analyses. Using GPEs as inexpensive approximations to
 367 the output of the code, together with the use of parallel computers, enables
 368 MC based analyses to be performed within reasonable time periods. The
 369 unconditional variance of the simulator output can be written as:

$$\mathbb{V}[Y] = \mathbb{E}[Y^2] - \mathbb{E}[Y]^2 \quad (11)$$

370 When using the emulator, the simulator output Y in Eq. (11) is substituted
 371 with the posterior mean of the emulator $\mathbb{E}[\eta(\mathbf{X})|\mathbf{y}]$ (Eq. (8)). Then, the
 372 Monte Carlo approximations of the terms in Eq. (11) are given by:

$$\hat{\mathbb{E}}[Y] = \frac{1}{N} \sum_{n=1}^N \mathbb{E}[\eta(\mathbf{x}^{(n)})|\mathbf{y}] \quad (12)$$

373

$$\hat{\mathbb{V}}[Y] = \frac{1}{N-1} \sum_{n=1}^N \mathbb{E}[\eta(\mathbf{x}^{(n)})|\mathbf{y}]^2 - \hat{\mathbb{E}}[Y]^2 \quad (13)$$

374 Here we only give the estimator for the first-order and the *total* conditional
 375 variances, since any higher-order variances could be calculated from their
 376 definitions in Eq. (2) and in Eq. (5).

$$\hat{\mathbb{V}}[\mathbb{E}[Y|X_i]] = \frac{1}{N-1} \sum_{n=1}^N \mathbb{E}[\eta(x_i^{(n)}, \mathbf{x}_{\sim i}^{(n)})|\mathbf{y}] \mathbb{E}[\eta(x_i^{(n)}, \mathbf{x}'_{\sim i}{}^{(n)})|\mathbf{y}] - \hat{\mathbb{E}}[Y]^2 \quad (14)$$

377

$$\hat{\mathbb{V}}[\mathbb{E}[Y|\mathbf{X}_{\sim i}]] = \frac{1}{N-1} \sum_{n=1}^N \mathbb{E}[\eta(x_i^{(n)}, \mathbf{x}'_{\sim i}{}^{(n)})|\mathbf{y}] \mathbb{E}[\eta(x_i'^{(n)}, \mathbf{x}_{\sim i}^{(n)})|\mathbf{y}] - \hat{\mathbb{E}}[Y]^2 \quad (15)$$

378 where \mathbf{x} and \mathbf{x}' come from two distinct sets of values for \mathbf{X} each of size
 379 $N \times d$. The full algorithm for the calculation of the first order and total
 380 Sobol' indices is given in [29]. In some instances, analytical expressions
 381 from the GPE are available for all quantities of interest, but these rely on

382 some modelling assumptions and hence we resort to sampling the posterior
383 of the GPE directly. A straightforward convergence study was carried out
384 to determine a suitable sample size. The procedure was based on obtaining
385 100 Sobol' index estimates based on 20 different sample sizes between $N =$
386 1000 and $N = 20\,000$. In Figure 5 we plot the mean and one standard
387 deviation of the first order indices for density and select the appropriate
388 sample size as the one after which there is no appreciable change in the
389 index' standard deviation. In this case the size was selected to be $N =$
390 10 000 points per variable. Inspecting Figure 6, which shows the same study
391 based on the total indices, confirms the correctness of the choice. A sample
392 of $N = 10\,000$ points per variable results in a total of $M = N \times (d + 2) =$
393 150 000 points for estimating first and total Sobol' indices for all 13 variables.
394 It is immediately obvious that such a sample could have not come directly
395 from the model at a reasonable computational cost. Figure 7 shows a set
396 of bar graphs representing the first order and total Sobol' indices of the 13
397 micromechanical parameters for density, longitudinal and transverse Young's
398 modulus, in rows (a) - (c), respectively. Figure 8 follows the same logic and
399 depicts the Sobol' index ranking for bending, compression and shear stiffness
400 in rows (a) - (c), respectively.

401 [Figure 5 about here.]

402 [Figure 6 about here.]

403 [Figure 7 about here.]

404 [Figure 8 about here.]

405 The indices represent a ratio of variances so they can not (in theory) be
406 negative. However some estimated values that are close to 0 are negative,
407 due to the fact that all integrals are estimated using sums (see Eq. (14)). It
408 is useful therefore to have a measure of confidence in the estimations.

409 Traditionally the use of *bootstrap* [30] has been employed when the data
410 generating process is expensive and limits the size of available observations;
411 see for instance [31]. When using the emulator however, this is not the case
412 and predictions for any given input combination are readily available. The
413 fact that the GPE is only an approximation to the output of the real code
414 can be accounted for by sampling the whole posterior distribution, instead of
415 just its mean. The error bars on Figures 7 and 8 depict ± 2 sample standard
416 deviations obtained from sampling the emulator 1000 times. These measures
417 give a 95% confidence interval for the indices and reflect the validity in the
418 predictions from the GPE shown in Figures 3 and 4

419 5. Discussion

420 Probabilistic sensitivity analysis used in conjunction with GPE provides
421 an affordable way of constructing Sobol' indices. Using this framework any
422 number of indices or combinations thereof can be easily computed. For prac-
423 tical (visualisation) reasons we only compute the first and total Sobol' indices.
424 We remind the reader that these two indicators measure the influence of the
425 micromechanical properties on the uncertain macroscopic response. Here, a
426 micromechanical parameter is considered to be non-influential (or with lit-
427 tle impact) on the macroscopic response if both Sobol' indices are zero (or
428 nearly zero). In general, the same trends in the first-order and total Sobol'

429 indices are observed in both Figures 7 and 8, which represents weak inter-
430 action among parameters. Interaction among input variables is indicated as
431 the relative increase in the total Sobol' indices as compared to the first order
432 terms. It is noted that this increase quantifies that part of the response vari-
433 ability which cannot be written off as a simple superposition of input effects.
434 Weak interactions is not to say that their relative magnitude with respect
435 to the corresponding first order effect is small, but rather that there are no
436 major changes in the ordering of the inputs by importance. The insets in
437 each figure show a magnification of those indices which can change order in
438 the overall importance ranking due to their quantified uncertainty. Most of
439 the affected parameters have relatively low Sobol' indices and are thus simply
440 a demonstrator of the fact that sensitivity ranking is a probabilistic measure
441 and should not be taken to have a fixed numerical value. For example the
442 inset in Figure 8(b) shows that the importance of the thickness of late wood
443 fibres can dominate that early wood fibres for compression stiffness. In gen-
444 eral, parameters that were identified as important kept their positions after
445 the inclusion of uncertainty. For the sake of clarity only two first order Sobol'
446 indices are show in the inset. On the other hand all total indices whose error
447 bars could not be clearly distinguished are shown in the insets in the left col-
448 umn of Figures 7 and 8. It is worth mentioning that the results presented in
449 Section 4 depend on the assumed parametric distribution (see Table 1). This
450 however, does not hold for the general methodology, which is independent of
451 the modelling assumptions and can be applied to a wide variety of problems.

452 A great influence of the cellulose content on the CLT stiffness parame-
453 ters K_{bend} , K_{comp} and K_{sh} is observed in Figures 8. The greatest influence

454 is produced by the cellulose volume fraction f_c on the in-plane shear CLT
455 stiffness K_{sh} , with a First order Sobol' index S_i^1 close to 0.36, and a total
456 Sobol' index S_i^T around 0.38. Furthermore, its influence on the CLT stiff-
457 ness is lower for the bending and compression deformation mechanisms (i.e.,
458 K_{bend} and K_{comp} , respectively), with S_i^1 and S_i^T just about 0.3 in both cases.
459 This can be attributed to the fact that during the in-plane shear deformation
460 process, the three CLT layers contribute greatly to the overall shear stiffness
461 of the CLT plate. Nevertheless, for the bending and compression deforma-
462 tion modes, only the two external CLT layers (whose wood fibres are aligned
463 with the loading direction) contribute significantly to the overall stiffness.
464 The central CLT layer provides little stiffness because the wood fibres are
465 perpendicular to the loading direction.

466 We note that the above strong influence of the cellulose content on the
467 overall stiffness was expected. Nevertheless, neither the difference between
468 the influence of the cellulose content on the shear deformation mode and on
469 the bending and compression behaviour, nor its numerical quantification, was
470 evident. This represents the main justification of carrying out the present
471 sensitivity analysis.

472 Other influencing parameters on the CLT stiffness components are the
473 *late-wood* and *early-wood* cell-wall thicknesses, t_{cv} and t_{cp} , respectively, with
474 first-order and total Sobol' indices around 0.2 for the compression and shear
475 stiffness, and t_{cp} over 0.25 for bending.

476 The influence of the microfibril angle, *MFA*, on the CLT stiffness is lower
477 than that produced by the cell-wall thickness parameters. Here, the total
478 Sobol' indices reach a maximum value of 0.07 for shear, 0.14 for compression

479 and 0.12 for bending, and first order indices of 0.03, 0.12 and 0.11 , respec-
480 tively. The remaining micromechanical parameters influence very little on
481 the CLT stiffness components.

482 As expected, the density ρ is strongly affected by the *late-wood* and *early-*
483 *wood* cell-wall thicknesses, and by the angle θ . Their corresponding total
484 indices exceed 0.37, 0.31 and 0.24, respectively. In particular, the strong
485 influence of *late-wood* is due to their thicker cell-walls when compared with
486 *early-wood* fibres. The influence of the remaining micromechanical parame-
487 ters on wood density can be neglected.

488 The influence on the longitudinal Young's modulus E_0 is mainly governed
489 by the degree of cellulose crystallinity f_{cc} , the cellulose volume fraction f_c ,
490 and by the angle MFA . Their corresponding total Sobol' indices are 0.29,
491 0.27 and 0.23, respectively. The *late-wood* and *early-wood* thicknesses, and
492 the angle θ also influence the longitudinal Young's modulus, but their indices
493 are lower. The first two have a total index of 0.11 with 0.08 for the third.

494 Contrary to E_0 , the transverse Young's modulus E_{90} is greatly influenced
495 by the *late-wood* cell-wall thickness, with first-order and total Sobol' indices
496 nearly 0.6. This behaviour can be attributed to the fact that E_{90} is mainly
497 governed by the cell-wall matrix's response. The little influence of the MFA
498 on E_{90} also contrasts with the great influence of MFA on E_0 . Here, both
499 Sobol' indices approach zero. Nevertheless, a greater influence on E_{90} could
500 eventually be found if the values of MFA were greater. However, the emulator
501 was trained with small values of $MFA \in [0^\circ-22^\circ]$.

502 The angle θ is another influencing parameter on E_{90} . Its corresponding
503 Sobol' indices are close to 0.2. This behaviour is explained by the fact that

504 the angle θ determines the transverse shape of wood fibres. Therefore, it also
505 affects the behaviour of E_{90} .

506 In general, the tangential and radial dimensions of wood fibres, T_p , T_v ,
507 R_p and R_v , have virtually no impact on the macroscopic response. Similarly,
508 the volume fraction of hemicellulose f_h , the length of the crystalline cellulose
509 fraction L_{cc} and the volume fraction of *early-wood* fibres with respect to the
510 total volume of growth ring P_{ew} , have also very little impact on the macro-
511 scale. The relevance of identifying these non-influencing parameters is that
512 they can be removed from the modelling process in order to develop simpler
513 and much more efficient models.

514 6. Conclusion

515 The influence of micromechanical properties of wood on its uncertain
516 macroscopic response was investigated by means of a probabilistic sensitiv-
517 ity analysis. A homogenisation-based multiscale approach was adopted to
518 capture the micro-macro relations existing in wood. Due to the relevance
519 within the engineering community, the influence on the structural response
520 of sawn wood and CLT plates was studied. The most influential microscopic
521 parameter on the CLT stiffness components was found to be the cellulose
522 content f_c . The degree of cellulose crystallinity, and the early and late wood
523 thicknesses also played an important role on the CLT stiffness. The hemi-
524 cellulose volume fraction, the tangential and radial dimensions of the wood
525 fibre and the length of the crystalline cellulose showed very little influence
526 on the macroscopic response. The volume fraction of early wood fibres with
527 respect to the total volume of growth rings also showed little effect on the

528 macroscopic stiffness. A practical insight into the definition of the microme-
529 chanical parameters allows to have an idea of the relevance of each parameters
530 in the determination of the macroscopic response after the homogenisation
531 procedure. Thanks to the sensitivity results presented in this work, the rel-
532 evance of the parameters can not only be verified, but also quantitatively
533 measured. These results are of practical interest, as they provide a simple
534 criterion to weight the micromechanical parameters for future optimization
535 of the macroscopic responses.

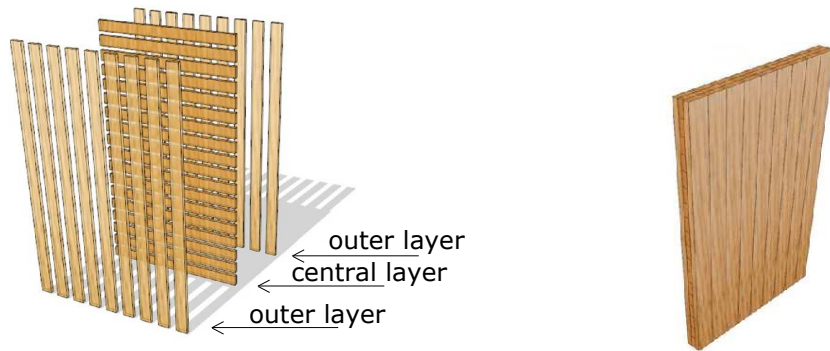
536 **Acknowledgments**

537 E.I. Saavedra Flores acknowledges the financial support from the Chilean
538 National Commission for Scientific and Technological Research (CONICYT),
539 FONDECYT REGULAR research project No 1160691.
540 P.O. Hristov acknowledges the funding provided by Parker-Hannifin Manu-
541 facturing (UK) Ltd.

542 **List of Figures**

543 1 Schematic representation of a CLT panel [32]. 28
544 2 Finite element meshes of the RVEs and structures analysed
545 in this paper along with their corresponding length scales.
546 (a) RVE associated with the *microfibril* scale (for the sake
547 of clarity, only one half of the RVE is shown here); (b) RVE
548 associated with the modelling of *late-wood* fibres; (c) RVE
549 associated with *early-wood* fibres; (d) growth ring RVE; (e) 4-
550 cm-thick layer subject to four-point bending; (f) 12-cm-thick
551 CLT panel (consisting of three 4-cm-thick layers). For the sake
552 of clarity, the FE mesh has been hidden. Figure adapted from
553 [32]. 29
554 3 Simulated versus emulated values. The prediction is given by
555 the posterior mean and the 95% credible interval (error bars)
556 is given by the posterior variance of the emulator. 30
557 4 Individual prediction errors for all six macro parameters. The
558 emulator value has a *Student-t* posterior distribution and the
559 errors should lie within the interval $[-2, 2]$ with 95% confidence. 31
560 5 Convergence study for the first order parameter effects on den-
561 sity. Line and error bars are mean and ± 1 standard deviation
562 of the indices distribution estimated by sampling the emulator
563 mean. 32
564 6 Convergence study for the total parameter effects on density.
565 Line and error bars are mean and ± 1 standard deviation of
566 the indices distribution estimated by sampling the emulator
567 mean. All non-influential values are overestimated at small
568 sample sizes. 33
569 7 First and total Sobol' indices for density, longitudinal and
570 transverse Young's moduli, (a) to (c), respectively. Error bars
571 show ± 2 standard deviations of the indices obtained from the
572 Gaussian process posterior. The insets show magnification of
573 some sets of indices which could change importance due to
574 errors. Refer to the text for more detail. 34

575	8	First and total Sobol' indices for bending, compression and	
576		shear stiffness, (a) to (c), respectively. Error bars show ± 2	
577		standard deviations of the indices obtained from the Gaussian	
578		process posterior. The insets show magnification of some sets	
579		of indices which could change importance due to errors. Refer	
580		to the text for more detail.	35



(a) Stacked layers.

(b) Glued layers.

Figure 1: Schematic representation of a CLT panel [32].

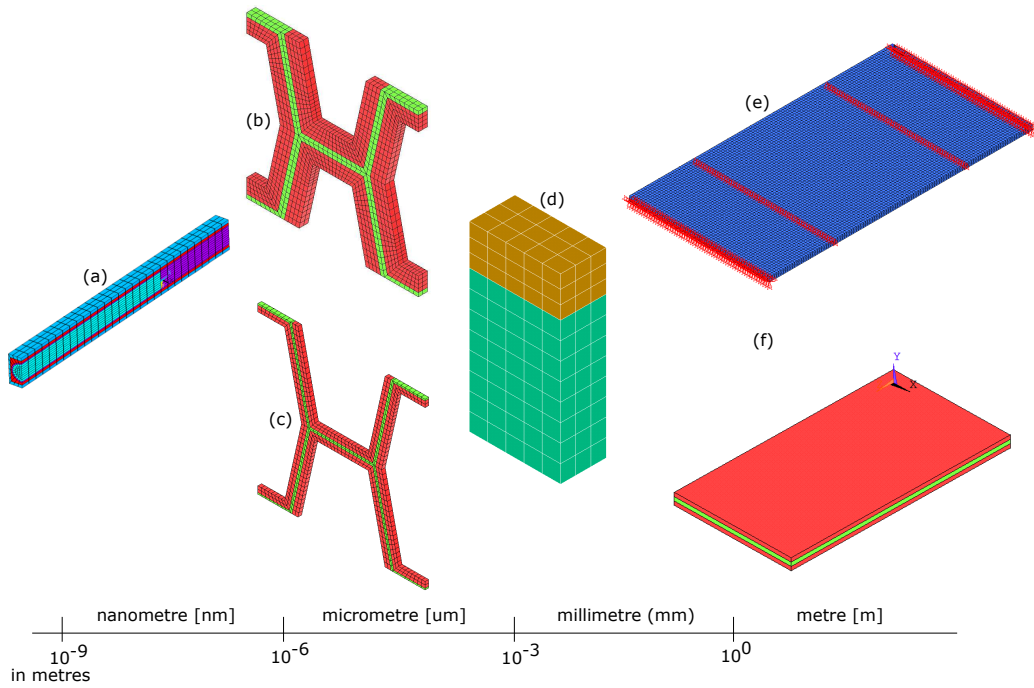


Figure 2: Finite element meshes of the RVEs and structures analysed in this paper along with their corresponding length scales. (a) RVE associated with the *microfibril* scale (for the sake of clarity, only one half of the RVE is shown here); (b) RVE associated with the modelling of *late-wood* fibres; (c) RVE associated with *early-wood* fibres; (d) growth ring RVE; (e) 4-cm-thick layer subject to four-point bending; (f) 12-cm-thick CLT panel (consisting of three 4-cm-thick layers). For the sake of clarity, the FE mesh has been hidden. Figure adapted from [32].

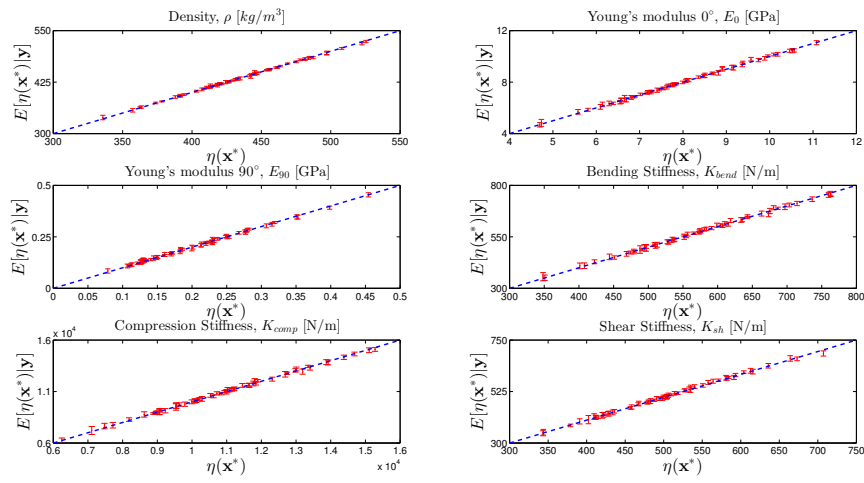


Figure 3: Simulated versus emulated values. The prediction is given by the posterior mean and the 95% credible interval (error bars) is given by the posterior variance of the emulator.

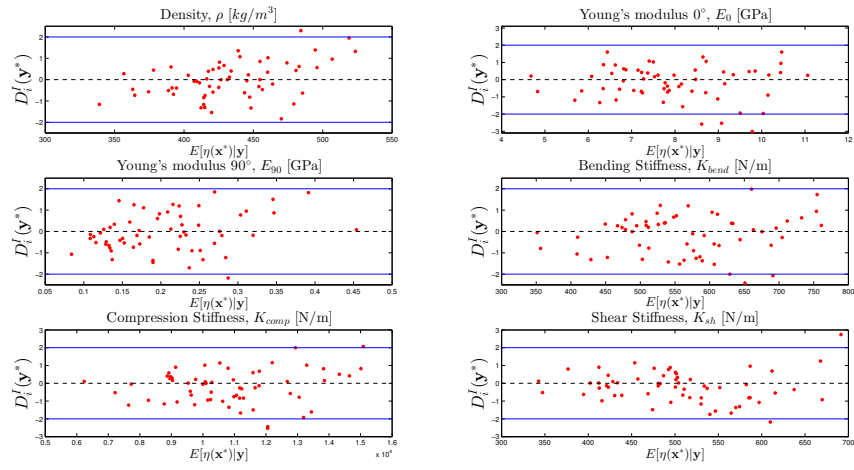


Figure 4: Individual prediction errors for all six macro parameters. The emulator value has a *Student-t* posterior distribution and the errors should lie within the interval $[-2, 2]$ with 95% confidence.

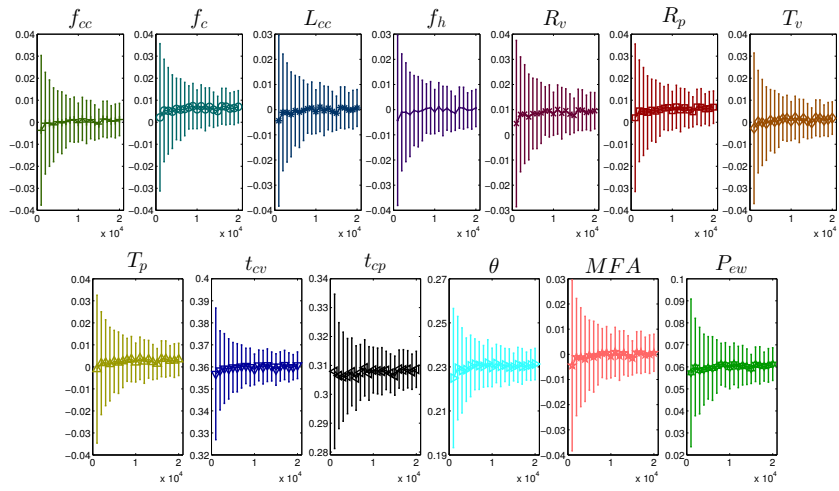


Figure 5: Convergence study for the first order parameter effects on density. Line and error bars are mean and ± 1 standard deviation of the indices distribution estimated by sampling the emulator mean.

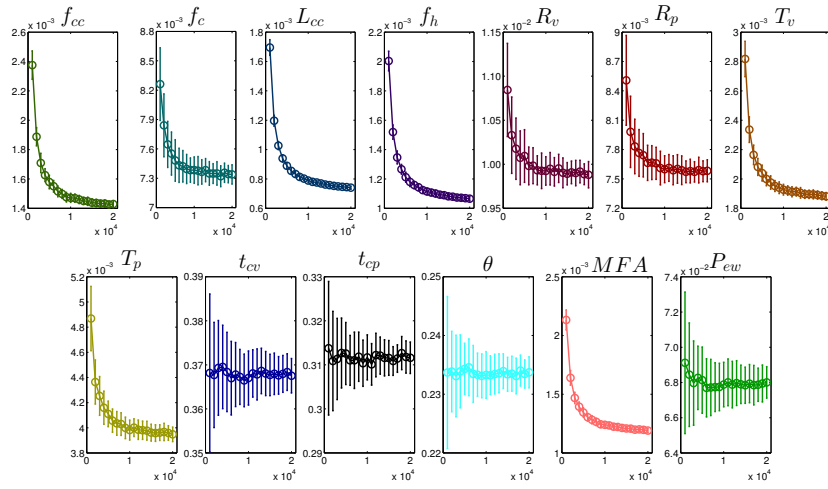
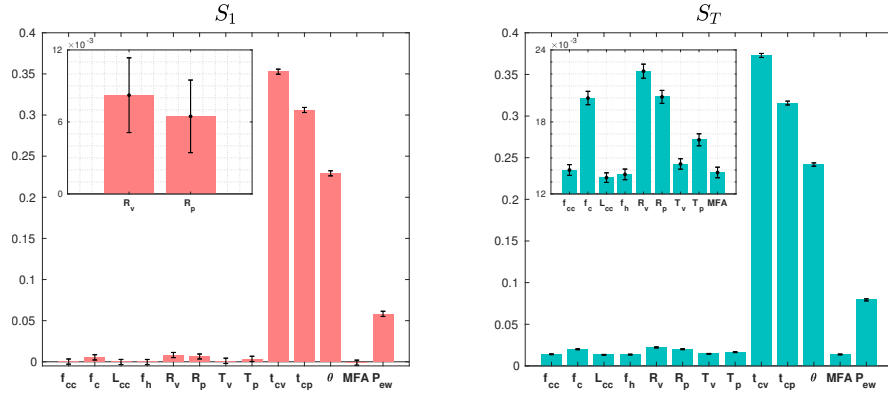
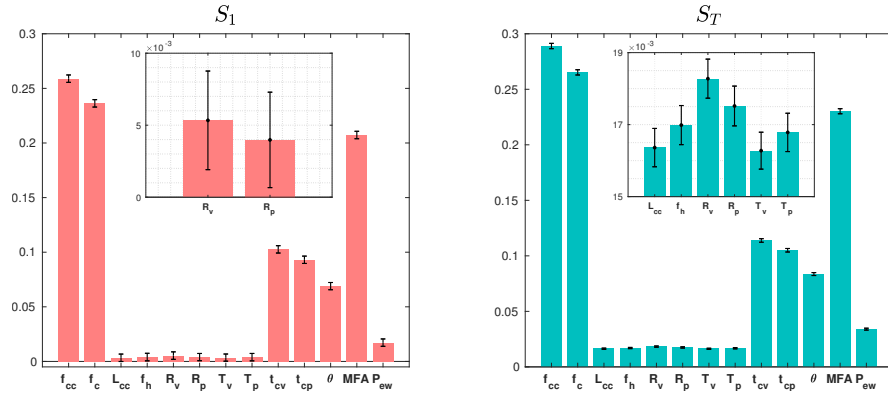


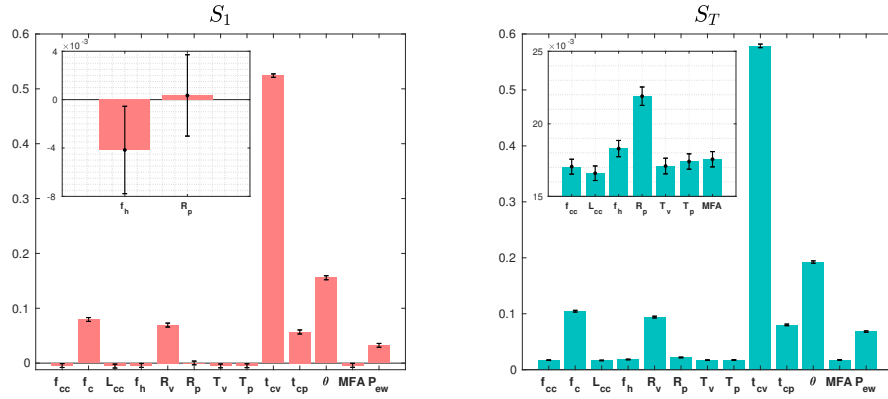
Figure 6: Convergence study for the total parameter effects on density. Line and error bars are mean and ± 1 standard deviation of the indices distribution estimated by sampling the emulator mean. All non-influential values are overestimated at small sample sizes.



(a) Density, ρ

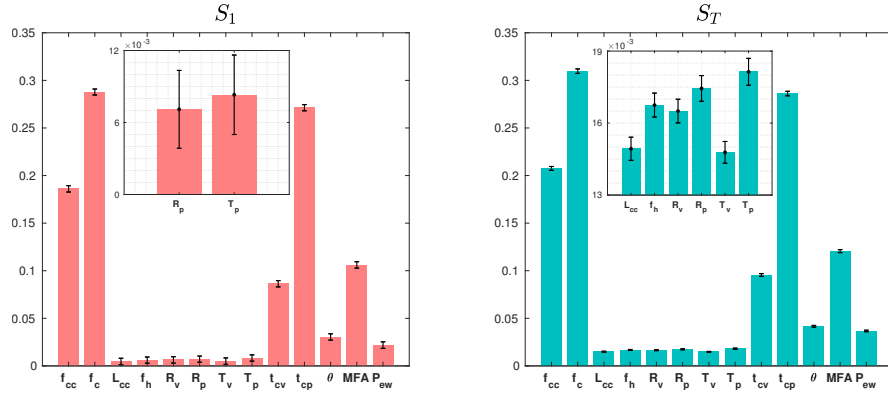


(b) Longitudinal Young's modulus, E_0

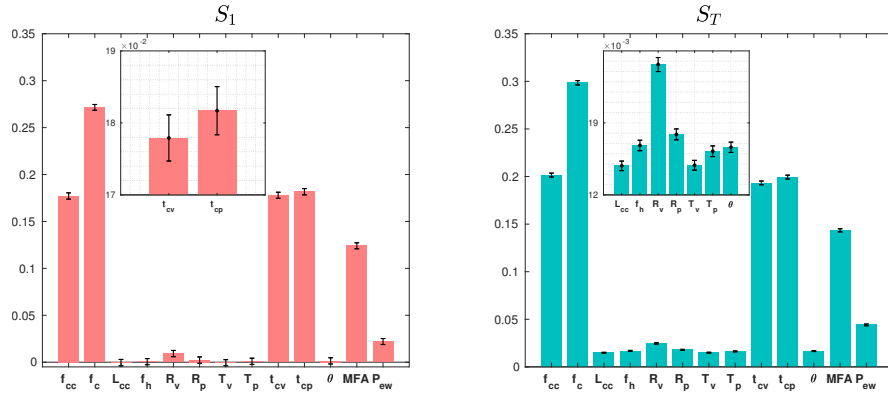


(c) Transverse Young's modulus, E_{90}

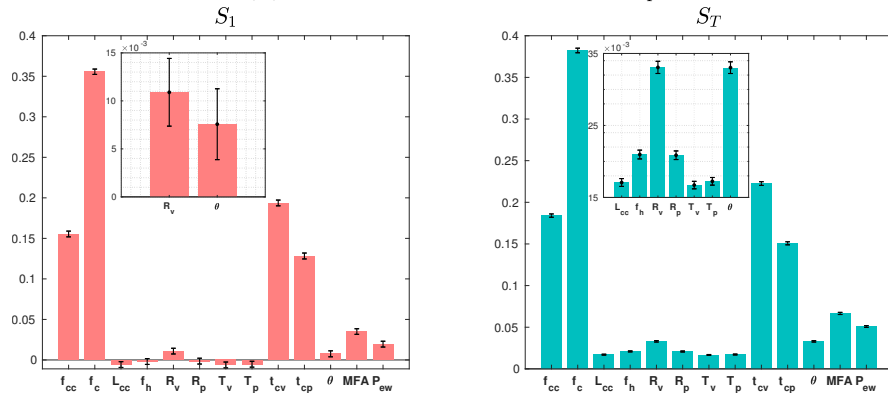
Figure 7: First and total Sobol' indices for density, longitudinal and transverse Young's moduli, (a) to (c), respectively. Error bars show ± 2 standard deviations of the indices obtained from the Gaussian process posterior. The insets show magnification of some sets of indices which could change importance due to errors. Refer to the text for more detail.



(a) Bending stiffness, K_{bend}



(b) Compression stiffness, K_{comp}



(c) Shear stiffness, K_{sh}

Figure 8: First and total Sobol' indices for bending, compression and shear stiffness, (a) to (c), respectively. Error bars show ± 2 standard deviations of the indices obtained from the Gaussian process posterior. The insets show magnification of some sets of indices which could change importance due to errors. Refer to the text for more detail.

581 **List of Tables**

582 1 Input parameter distribution - $U(a, b)$ 37

Table 1: Input parameter distribution - $U(a, b)$.

	f_{cc}	f_c	L_{cc}	f_h	R_v	R_p	T_v	T_p	t_{cv}	t_{cp}	θ	MFA	P_{ew}
	%	%	nm	%	μm	μm	μm	μm	μm	μm	deg	deg	%
a	0.45	0.30	26.50	0.25	31.00	37.00	25.00	28.00	4.30	3.10	10.00	0.00	0.67
b	0.60	0.50	36.40	0.29	37.00	40.00	27.00	30.00	8.00	4.30	27.50	22.00	0.80

- 583 [1] W. Munoz, M. Mohammad, S. Gagnon, Lateral and withdrawal resis-
584 tance of typical CLT connections, in: A. Ceccotti (Ed.), Proceedings of
585 the 11th World Conference on Timber Engineering (WCTE), Trentino,
586 Italy, 2010.
- 587 [2] E. I. Saavedra Flores, K. Saavedra, J. Hinojosa, Y. Chandra, R. Das,
588 Multi-scale modelling of rolling shear failure in cross-laminated timber
589 structures by homogenisation and cohesive zone models, *International*
590 *Journal of Solids and Structures* 81 (2016) 219 – 232.
- 591 [3] J. C. Michel, H. Moulinec, P. Suquet, Effective properties of compos-
592 ite materials with periodic microstructure: a computational approach,
593 *Computer Methods in Applied Mechanics and Engineering* 172 (1999)
594 109–143.
- 595 [4] M. Oudjene, E.-M. Meghlat, H. Ait-Aider, J.-L. Batoz, Non-linear fi-
596 nite element modelling of the structural behaviour of screwed timber-
597 to-concrete composite connections, *Composite Structures* 102 (2013) 20
598 – 28.
- 599 [5] V.-D. Tran, M. Oudjene, P.-J. Mausooone, Experimental and numerical
600 analyses of the structural response of adhesively reconstituted beech
601 timber beams, *Composite Structures* 119 (2015) 206 – 217.
- 602 [6] M. Osei-Antwi, J. de Castro, A. P. Vassilopoulos, T. Keller, Modeling
603 of axial and shear stresses in multilayer sandwich beams with stiff core
604 layers, *Composite Structures* 116 (2014) 453 – 460.

- 605 [7] C. OLoinsigh, M. Oudjene, E. Shotton, A. Pizzi, P. Fanning, Mechanical
606 behaviour and 3d stress analysis of multi-layered wooden beams made
607 with welded-through wood dowels, *Composite Structures* 94 (2) (2012)
608 313 – 321.
- 609 [8] E. I. Saavedra Flores, F. A. DiazDelaO, M. I. Friswell, R. M. Ajaj,
610 Investigation on the extensibility of the wood cell-wall composite by an
611 approach based on homogenisation and uncertainty analysis, *Composite*
612 *Structures* 108 (2014) 212–222.
- 613 [9] E. I. Saavedra Flores, F. A. DiazDelaO, R. M. Ajaj, M. I. Friswell, G. F.
614 Fernando, Mathematical modelling of the stochastic mechanical proper-
615 ties of wood and its extensibility at small scales, *Applied Mathematical*
616 *Modelling* 38 (15–16) (2014) 3958–3967.
- 617 [10] A. Forrester, A. Sobester, A. Keane, *Engineering design via surrogate*
618 *modelling: A practical guide*, Wiley, 2008.
- 619 [11] E. I. Saavedra Flores, I. Dayyani, R. Ajaj, R. Castro-Triguero, F. Di-
620 azDelaO, R. Das, P. González Soto, Analysis of cross-laminated timber
621 by computational homogenisation and experimental validation, *Com-*
622 *posite Structures* 121 (2015) 386 – 394.
- 623 [12] P. Fratzl, I. Burgert, J. Keckes, Mechanical model for the deformation
624 of the wood cell wall, *Zeitschrift für Metallkunde / Materials Research*
625 *and Advanced* 7 (95) (2004) 579–584.
- 626 [13] J. Dinwoodie, *Timber – Its nature and behavior*, Von Nostrand Rein-
627 *hold*, New York, 1981.

- 628 [14] J. Bodig, B. Jayne, Mechanics of wood and wood composites, Von Nos-
629 trand Reinhold, New York, 1982.
- 630 [15] INN – Instituto Nacional de Normalización, NCh 801. Of. 2003. elemen-
631 tos de construcción -Paneles- Ensayo de carga compresión, Chile.
- 632 [16] INN – Instituto Nacional de Normalización, NCh 802. EOf. 1971. Ar-
633 quitectura y construcción - Paneles prefabricados - Ensayo de carga hor-
634 izontal, Chile.
- 635 [17] INN – Instituto Nacional de Normalización, NCh 803. Of. 2003. elemen-
636 tos de construcción - Paneles - Ensayo de carga flexión, Chile.
- 637 [18] C. Miehe, J. Shotte, M. Lambrecht, Homogenization of inelastic solid
638 materials at finite strains based on incremental minimization principles.
639 application to the texture analysis of polycrystals, Journal of the Me-
640 chanics and Physics of Solids 50 (10) (2002) 2123–2167.
- 641 [19] R. Castro-Triguero, E. Garcia-Macias, E. I. Saavedra Flores, M. I.
642 Friswell, R. Gallego, Multi-scale model updating of a timber footbridge
643 using experimental vibration data, Engineering Computations 34 (3)
644 (2017) 754–780.
- 645 [20] ANSYS, Parametric Design Language Guide. Release 16.1, ANSYS, Inc.,
646 Canonsburg, PA 15317, <http://www.ansys.com>, 2016.
- 647 [21] A. Saltelli, M. Ratto, T. Andres, F. Campolongo, J. Cariboni, D. Gatelli,
648 M. Saisana, S. Tarantola, Global sensitivity analysis. The primer, John
649 Wiley & Sons, 2008.

- 650 [22] I. M. Sobol, Global sensitivity indices for nonlinear mathematical mod-
651 els and their Monte Carlo estimates, *Mathematics and Computers in*
652 *Simulation* 55 (1-3) (2001) 271–280.
- 653 [23] T. Homma, A. Saltelli, Importance measures in global sensitivity analy-
654 sis of nonlinear models, *Reliability Engineering & System Safety* 52 (1)
655 (1996) 1–17.
- 656 [24] A. Saltelli, S. Tarantola, F. Campolongo, M. Ratto, *Sensitivity analysis*
657 *in practice: A guide to assessing scientific models*, Wiley, 2004.
- 658 [25] J. Bernardo, A. Smith, *Bayesian theory*, *Wiley Series in Probability &*
659 *Statistics*, Wiley, 1994.
- 660 [26] J. Oakley, *Bayesian uncertainty analysis for complex computer codes*,
661 *Ph.D. thesis*, University of Sheffield (1999).
- 662 [27] W. Becker, *Uncertainty propagation through large nonlinear models*,
663 *Ph.D. thesis*, University of Sheffield (2011).
- 664 [28] L. S. Bastos, A. OHagan, Diagnostics for Gaussian process emulators,
665 *Technometrics* 51 (4) (2009) 425–438.
- 666 [29] A. Saltelli, Making best use of model evaluations to compute sensitivity
667 indices, *Computer Physics Communications* 145 (2) (2002) 280–297.
- 668 [30] B. Efron, R. J. Tibshirani, *An introduction to the bootstrap*, CRC press,
669 1994.

- 670 [31] G. E. B. Archer, A. Saltelli, I. M. Sobol, Sensitivity measures, ANOVA-
671 like techniques and the use of bootstrap, *Journal of Statistical Compu-*
672 *tation and Simulation* 58 (2) (1997) 99–120.
- 673 [32] E. I. Saavedra Flores, R. M. Ajaj, I. Dayyani, Y. Chandra, R. Das,
674 Multi-scale model updating for the mechanical properties of cross-
675 laminated timber, *Computers and Structures* 177 (2016) 83 – 90.